Peer-reviewed version available at *Minerals* **2018**, *8*, 287; doi:10.3390/min8070287

REE and Y Mineralogy of the Krudum Granite Body (Saxothuringian Zone)

Miloš René

Institute of Rock Structure and Mechanics, v.v.i., Academy of Sciences of the Czech Republic, V Holešovičkách 41, Prague 8, 182 09, Czech Republic

Correspondence: rene@irsm.cas.cz; Tel.: +420-266-009-228

Abstract: The Krudum granite body comprises highly fractionated granitic rocks ranging from medium-F biotite granites to high-F, high-P_2O_5 Li-mica granites. This unique assemblage is an ideal site to continue recent efforts in petrology to characterize the role of zircon, monazite and xenotime as hosts to REEs. The granitic rocks of the Krudum body analysed in this study were found to contain variable concentrations of monazite and zircon, while xenotime was only found in the high-F, high-P_2O_5 Li-mica granites and in the alkali-feldspar syenites of the Vysoký Kámen stock. For analysed monazites of all magmatic suites cheralite substitution was significant. The highest concentration of cheralite was found in monazites from the high-F, Li-mica granites and from the alkali-feldspar syenites. The proportion of YPO_4 in all analysed xenotimes ranges from 71 to 84 mol. %. Some xenotimes were found to be hydrated and the observed water content estimated from analytical data ranged from 5 to 11 wt. % H_2O.

Peer-reviewed version available at Minerals 2018, 8, 287; doi:10.3390/min8070287

Analysed xenotimes were commonly enriched in HREEs (9.3– 19.5 wt. % $HREE_2O_3$) and thorite-coffinite and cheralite exchange was observed. Analysed zircons from granite suites of the Krudum granite body contained moderate Hf concentrations (1.0–4.7 wt. % HfO_2; 0.010–0.047 apfu Hf). The highest concentrations of HfO_2 were found in zircons from the high-F, high P_2O_5 Li-mica granites (1.2–4.7 wt. % HfO_2) and from the alkali-feldspar syenites (1.3–4.1 wt. % HfO_2). Zircons from the high-F, high-P_2O_5 Li-mica granites were often hydrated and fluorised. The concentrations of F in zircon from partly greisenised high-F, high-P_2O_5 Li-mica granites reached up to 1.2 wt. % (0.26 apfu F). In zircons from the alkali-feldspar syenites enrichment in P, which is not associated with a simultaneous enrichment in Y + REE, was also observed. Analysed zircons from the high-F, high P_2O_5 Li-mica granites were enriched in Y (up to 5.5 wt. % Y_2O_3; 0.10 apfu Y) and Sc (up to 1.17 wt. % Sc_2O_3; 0.03 apfu Sc).

Keywords: monazite; xenotime; zircon; granite; Bohemian Massif; Horní Slavkov; Karlovy Vary

1. Introduction

In the last ten years, several studies have emphasized the role of monazite, xenotime and zircon as major hosts for rare earth elements (REE) and Y in

Peer-reviewed version available at Minerals 2018, 8, 287; doi:10.3390/min8070287

granites [1–8]. However, several factors controlled composition of above mentioned accessory minerals remain unclear. To expand on this knowledge, unique assemblages of some highly fractionated granites in the Karlovy Vary pluton were selected for further analyses on these minerals.

The presented study concentrates on petrological and geochemical observations connected to the occurrence of monazite, xenotime and zircon in compositionally different granites of the Krudum granite body. This granite body is a subsidiary intrusion of the Karlovy Vary pluton in the Slavkovský Les Mts. and is suitable for such a study according to its very interested fractionation of the medium-F biotite, high-F, high-P_2O_5 muscovite-biotite and Li-mica granites, accompanied by alkali feldspar syenites. The majority of granites found in this granite assemblage are highly fractionated granites of the Krušné Hory/Erzgebirge batholith with different concentrations of topaz, Li-mica and Sn-W-Nb-Ta minerals.

2. Geological setting

The Karlovy Vary pluton forms the southern edge of the Western Erzgebirge pluton that is part of the Variscan Krušné Hory/Erzgebirge batholith in western part of the Bohemian Massif [9–11]. This batholith consists of three individual plutons: Western, Middle and Eastern, each

representing an assembly of shallowly emplaced granite units about 6–10 km paleodepth, with a maximum preserved vertical thickness of the pluton 10–13 km below the present surface level [11–12]. The batholith belongs to one coherent and cogenetic, ca. 400 km long plutonic megastructure of the Saxo-Danubian Granite Belt [13].

Geochemically, five groups of granites were previously distinguished in the Krušné Hory/Erzgebirge batholith: (i) low-F biotite granites, (ii) low-F two-mica granites, (iii) high-F, high P_2O_5 Li-mica granites, (iv) high-F, low-P_2O_5 Li-mica granites and (v) medium-F biotite granites [9-10]. In addition to the previously identified granite type (iii) high-F, high P_2O_5 Li-mica granites [10], this study divided this granite type into a muscovite-biotite high-F, high P_2O_5 granites (vi) and own high-F, high-P_2O_5 Li-mica granites. Additionally was found quartz-free alkali-feldspar syenite (vii), which forms a distinct separate part of the Vysoký Kámen stock. The Western Krušné Hory/Erzgebirge pluton is interpreted as a sequence of separately emplaced magma batches or an assemblage of several magmatic pulses, emplaced more or less contemporaneously [9-10, 14]. The outcrops of this pluton could be divided into the Nejdek–Eibenstock and Karlovy Vary plutons [11, 15].

Peer-reviewed version available at Minerals 2018, 8, 287; doi:10.3390/min8070287

The Krudum granite body (KGB, c. 50 km^2) on the southwestern margin of the Karlovy Vary pluton (KVP) shows a concentric structure (Figure 1).

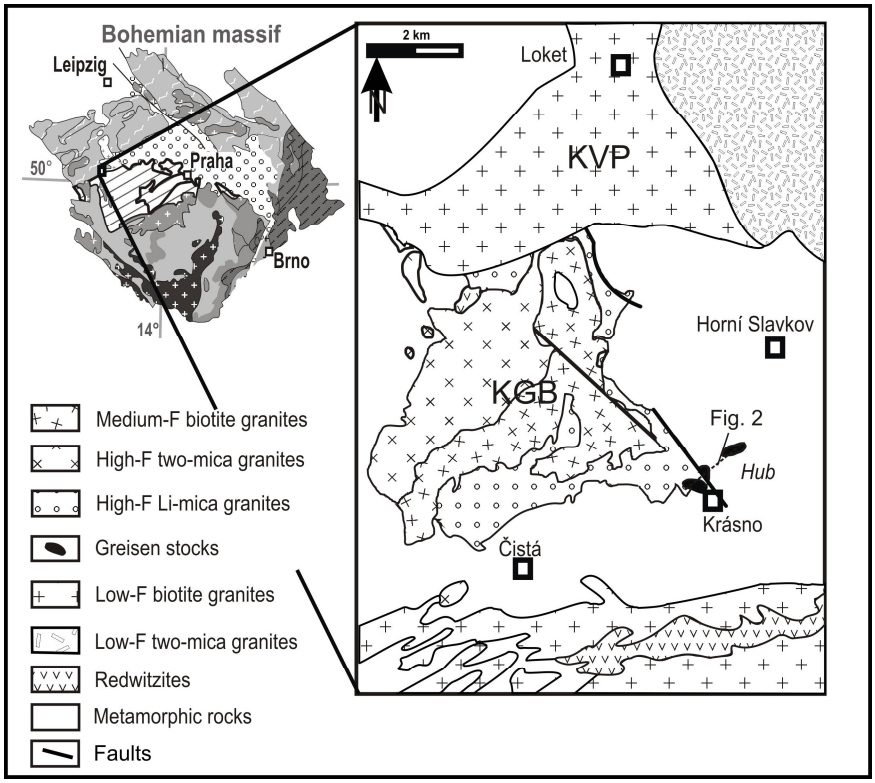

Figure 1 Schematic geological map of the Krudum granite body.

Porphyritic medium-F biotite granites, surrounded to the NW by younger, high-F, high-P_2O_5 topaz-bearing muscovite-biotite granites, form its centre. The youngest, high-F, high-P_2O_5 Li-mica granite forms the outermost shell [16]. The inner structure of the south-eastern edge of the KGB, partly overlain by metamorphic rocks of the Slavkov crystalline unit, is well

stratified, comprising variable greisenised high-F, high-P_2O_5 Li-mica granites occurring also in the Hub and Schnöd greisen stocks hosting a world-famous Sn-W-Nb-Ta-Li mineralisation of the Horní Slavkov-Krásno ore district [16–20] (Figure 2).

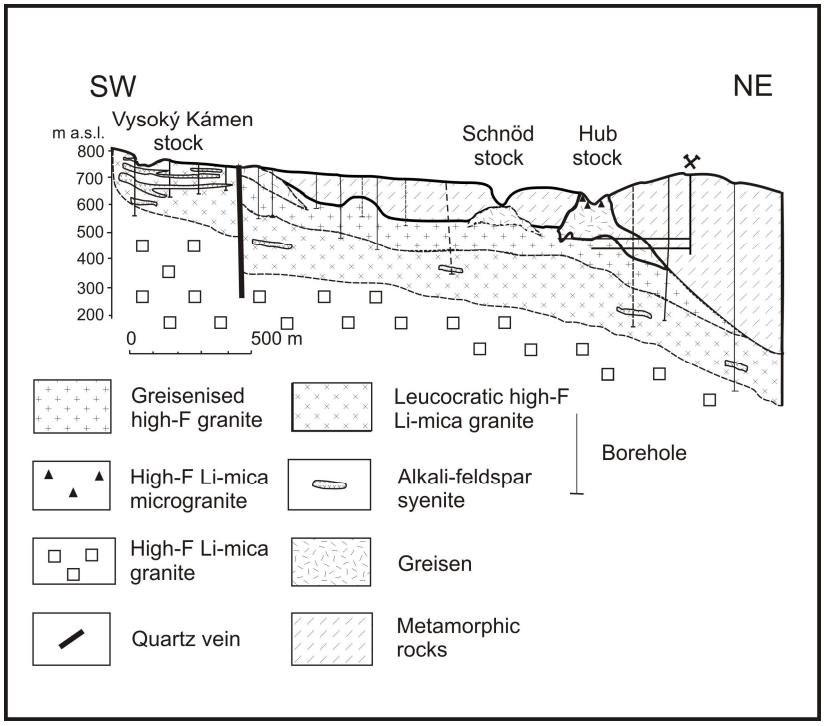

Figure 2 Geological cross section of the Horní Slavkov-Krásno ore district, after [17], modified by author.

3. Analytical methods

The whole rock composition of selected granitoids was analysed in a total of 66 samples. Rock samples of 2–5 kg weight were crushed in a jaw crusher

Peer-reviewed version available at Minerals 2018, 8, 287; doi:10.3390/min8070287

and a representative split of this material was ground to fine powder in an agate ball mill, before being pressed into XRF-tabs. Major elements were determined using a Pananalytical Axios Advanced fluorescence (XRF) spectrometer at Activation Laboratories Ltd., Ancaster, Canada. The content of FeO was determined by titration, and H_2O^+ and H_2O^- were analysed gravimetrically. Trace elements were quantified by inductively coupled plasma mass spectrometry (ICP MS) techniques, also at Activation Laboratories Ltd., Ancaster, Canada, using a Perkin Elmer Sciex ELAN 6100 ICP mass spectrometer, following standard lithium metaborate/tetraborate fusion and acid decomposition sample preparation procedures. All analyses were calibrated against international reference materials.

Approximately 230 quantitative electron probe microanalyses of monazite, xenotime and zircon were performed in representative samples of all magmatic suites. Minerals were analysed in polished thin sections and back-scattered electron images (BSE) were acquired to study interaction of examined accessory minerals and the internal structure of individual mineral grains. Element abundances of Al, Ca, Ce, Dy, Er, Eu, F, Fe, Gd, Ho, La, Lu, Mg, Mn, Na, Nd, P, Pb, Pr, Sc, Si, Sm, Sr, Tb, Th, Ti, Tm, U, Y, Yb and

Peer-reviewed version available at Minerals 2018, 8, 287; doi:10.3390/min8070287

Zr in selected accessory minerals were determined using a CAMECA SX 100 electron probe micro-analyser (EPMA) operated in wavelength-dispersive mode. The contents of the above mentioned elements were determined using an accelerating voltage and beam current of 15 keV and 20 nA, respectively, with a beam diameter of 2–5 µm. The following standards, X-ray lines, and crystals (in parentheses) were used: AlK_α – sanidine (TAP), CaK_α – fluorapatite (PET); CeL_α – $CePO_4$ (PET); DyL_α – $DyPO_4$ (LIF); ErL_α – $ErPO_4$ (PET); EuL_β – $EuPO_4$ (LIF); FeK_α – almandine (LIF); GdL_β – $GdPO_4$ (LIF); HoL_β – $HoPO_4$ (LIF), LaL_α – $LaPO_4$ (PET), LuM_β – LuAG (TAP), MgK_α – Mg_2SiO_4 (TAP), MnK_α – spessartine (LIF), NdL_β – $NdPO_4$ (LIF); PK_α – fluorapatite (PET), PbM_α – vanadinite (PET); PrL_β – $PrPO_4$ (LIF), SrL_α – $SrSO_4$ (TAP), ScK_α – ScP_5O_{14} (PET); SiK_α – sanidine (TAP); SmL_β – $SmPO_4$ (LIF); TbL_α –$TbPO_4$ (LIF), ThM_α – $CaTh(PO_4)_2$ (PET), TiK_α – anatas (PET), TmL_α – $TmPO_4$ (LIF), UM_β – metallic U (PET), YL_α – YPO_4 (PET) and ZrL_α – zircon (TAP). Intra-REE overlaps were partially resolved using L_α and L_β lines. Empirically determined coincidences were applied after analysis: ThM_α on PbM_α and $ThM\gamma$ on the UM_β line. The raw data were converted into concentrations using appropriate PAP-matrix corrections [21]. The detection limits were

Peer-reviewed version available at Minerals 2018, 8, 287; doi:10.3390/min8070287

approximately 400 ppm for Y, 180–1700 ppm for REE and 800–1000 ppm for U and Th. Mole fractions for components in monazite and xenotime were calculated according to Pyle et al. [22].

4. Results

4.1 Petrography

The medium-F biotite granite (v) is porphyritic, fine-grained rock consisting perthitic potassium feldspar, plagioclase ($An_{0–31}$), quartz, abundant biotite flakes (annite, ^{IV}Al 2.15–2.30 atoms per formula unit, apfu, Ti 0.37–0.55 apfu, Fe/Fe+Mg 0.56–0.80) and rare muscovite. Fluorapatite, zircon, monazite-(Ce), magnetite and ilmenite are common accessory minerals.

The high-F, high-P_2O_5 topaz-bearing muscovite-biotite granite (vi) is equigranular, medium-grained rock with abundant coarsely flaky muscovite. In addition to perthitic potassium feldspar it contains plagioclase ($An_{0–12}$), quartz, biotite (annite, ^{IV}Al 2.12–2.39 apfu, Ti 0.26–0.39 apfu, Fe/Fe+Mg 0.72–0.76) muscovite and topaz. Common accessory minerals are apatite, zircon, monazite and ilmenite.

The high-F, high-P_2O_5 Li-mica granite (iii) is represented by more petrographic varieties, which could be classified as partly greisenised medium grained, equigranular granites, porphyritic, fine-grained granites

Peer-reviewed version available at Minerals 2018, 8, 287; doi:10.3390/min8070287

and leucocratic granites that occurs mainly in the Vysoký Kámen stock. The main granite variety is represented by medium-grained, equigranular rock, consisting of quartz, albite ($An_{0–2}$), potassium feldspar, lithium mica and topaz. Fluorapatite, zircon, Nb-Ta-Ti oxides, xenotime-(Y), monazite-(Ce), uraninite and coffinite are common accessory minerals. Cassiterite occurs usually as a very rare accessory mineral. Porphyritic, weakly greisenised granites occur as relatively small lenses or layers in the main granite body of equigranular Li-mica granites. Their groundmass is fine-grained with phenocrysts of potassium feldspar. Granites contain quartz, albite (An_{0-5}), potassium feldspar, Li-mica and topaz. Apatite, zircon, Nb-Ta-Ti oxides, xenotime-(Y) and monazite-(Ce) are common accessories. The second sub-type of this granite, the leucocratic granite occurring in the Vysoký Kámen stock, is mostly composed of albite (An_{0-2}), potassium feldspar, quartz and subordinate amounts of lithium mica and topaz. Fluorapatite, Nb-Ta-Ti oxides, fluorite and rare beryl represent accessories. Quartz-free alkali-feldspar syenite (vii), composed exclusively of albite and potassium feldspar, also forms subhorizontal layers and lenses ranging from several decimetres to tens of meter in thickness in the Vysoký Kámen stock. Its contacts with leucocratic granite are typically diffuse. The alkali-feldspar

Peer-reviewed version available at Minerals 2018, 8, 287; doi:10.3390/min8070287

syenite consists of albite ($An_{0–2}$), potassium feldspar, accessory lithium mica and topaz. Fluorapatite, triplite, Nb-Ta-Ti oxides, zircon, xenotime-(Y), monazite-(Ce) and very rare Nb-bearing wolframite are accessories. The alkali-feldspar syenite is described as feldspathite in some papers (e.g. [16–17]), but this name does not agree with the magmatic nature of this rock, which is in some places underlined by its striking magmatic layering (Figure 3).

Figure 3 Magmatic layering of alkali-feldspar syenite, Vysoký Kámen stock.

Peer-reviewed version available at Minerals 2018, 8, 287; doi:10.3390/min8070287

4.2 Geochemistry

The medium-F biotite granite (v) is weakly peraluminous Ca-poor granite with aluminium saturation index (ASI) ranging from 1.1 to 1.2. In comparison with common Ca-poor granites [23] it is enriched in Rb (455–589 ppm), Cs (40–52 ppm), Sn (24–44 ppm) and Nb (21–23 ppm), but poor in Mg (0.2–0.3 wt. % MgO), Ca (0.4–0.8 wt. % CaO), Sr (25–64 ppm), Ba (133–207 ppm), Zr (101–170 ppm) and Y (25–31 ppm).

The high-F granite, high-P_2O_5 muscovite-biotite granite (vi) is peraluminous Ca-poor S-type granite with ASI ranging from1.2 to 1.3. In comparison with common S-type granites [23] it is enriched in Li (78–546 ppm), Rb (393–936 ppm), Cs (30–169 ppm), Sn (8–50 ppm) and Nb (15–32 ppm), but poor in Mg (0.2–0.4 wt. % MgO), Ca (0.3–0.7 wt. % CaO), Sr (20–91 ppm), Ba (25–394 ppm), Zr (47–111 ppm) and Y (15-34 ppm).

The high-F, high-P_2O_5 Li-mica granite (iii) is highly a peraluminous S-type granite with ASI ranging from1.2 to 1.5. In comparison with typical S-type granites [23], it is enriched in incompatible elements such as Li (311–1050 ppm), Rb (830–1150 ppm), Cs (47–121 ppm), Sn (28–159 ppm), Nb (18–52 ppm), Ta (8–26 ppm) and W (3–66 ppm), but poor in Mg (0.1–0.4 wt. %

Peer-reviewed version available at Minerals 2018, 8, 287; doi:10.3390/min8070287

MgO), Ca (0.4–0.7 wt. % CaO), Sr (10-29 ppm), Ba (6–81 ppm), Zr (24–55 ppm) and (Y 5–17 ppm).

The leucocratic granite sub-type from the Vysoký Kámen stock is peraluminous S-type granite with ASI ranging from 1.1 to 1.3. In comparison with high-F, high-P_2O_5, Li-mica granite is partly enriched in Rb (670–1309 ppm), Nb (26–67 ppm) and Ta (15–33 ppm), but poor in Mg (0.04–0.11 wt. % MgO), Ca (0.3–0.6 wt. % CaO), Ba (8–25 ppm), Zr (13–26 ppm) and Y (3–7 ppm).

The alkali-feldspar syenite (vii) is weakly peraluminous rock with ASI ranging from 1.0 to 1.1. Relative to the high-F, high-P_2O_5 Li-mica granites, the syenite is enriched in Na (4.6–6.8 wt. % Na_2O), K (6.9–7.8 wt. % K_2O) Rb (1760–1800 ppm), Nb (14–60 ppm) and Ta (11–44 ppm), but depleted in Si (64.0–66.5 wt. % SiO_2), Mg (0.03–0.07 wt. % MgO), Ca (0.3–0.5 wt. % CaO), Zr (14–37 ppm) and Y (2–9 ppm).

The highest ΣREE was found in the medium-F biotite granites (v) (108–168 ppm) and in the high-F granites, high-P_2O_5 muscovite-biotite granites (vi) (91–175 ppm). In the high-F, high-P_2O_5 Li-mica granites (iii) and alkali-feldspar syenites (vii) the ΣREE are distinctly lower (3–46 ppm). For the medium-F biotite granites (v) and the high-F, high-P_2O_5 muscovite-biotite

Peer-reviewed version available at Minerals 2018, 8, 287; doi:10.3390/min8070287

granites (vi) the higher La/Yb ratios are significant (medium-F granites 4.3–7.2, high-F, high P_2O_5 muscovite-biotite granites 4.0–8.0), whereas the La/Yb ratios in the high-F, high-P_2O_5 granites (iii, iv) and alkali-feldspar syenites (vii) are lower (high-F, high P_2O_5 Li-mica granites 1.6–4.8, leucocratic granites 1.2–2.5. alkali-feldspar syenites 1.6–4.1). Similar differences exists also in the Eu/Eu* ratio (medium-F biotite granites 0.18–0.29, high-F, high P_2O_5 muscovite-biotite granites 0.21–0.31, high-F, high P_2O_5 Li-mica granites 0.03–0.32, leucocratic granites 0.04–0.13, alkali-feldspar syenites 0.02–0.17).

4.3. REE and Y mineralogy

4.3.1. Crystallisation sequences of monazite, xenotime and zircon

In the granite suites of the KGB rare earth element- (REE) and Y-bearing accessory minerals are represented by monazite, xenotime and zircon. Monazite and zircon occur in all magmatic suites, whereas xenotime was found only in the high-F, high-P_2O_5 Li-mica granites (iii) and in the alkali-feldspar syenites (vii). Monazite, together with zircon and fertile apatite is usually enclosed in biotite and lithium mica flakes. Monazite occurs as small subhedral to anhedral grains (10-30 μm), often grow together with zircon and or in complex aggregates together with coffinite and xenotime

(Figure 4). Monazite grains are usually without any zoning, for zircon is usually complex zoning significant. The xenotime occurs either as grains on the zircon rims or inclusions/intergrowths in bigger zircon crystals (Figure 5).

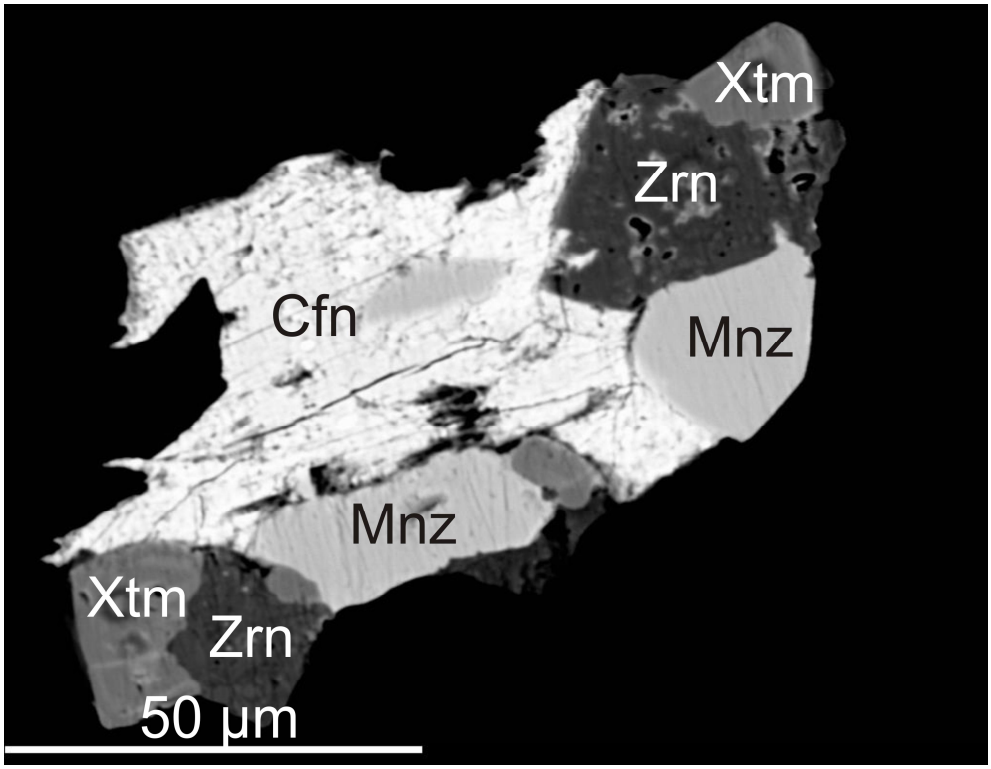

Figure 4 High contrasts BSE image of complex intergrowths of coffinite (Cfn), zircon (Zrn), monazite (Mnz) and xenotime (Xtm) from high-F, high-P_2O_5 Li-mica granite, Hub stock.

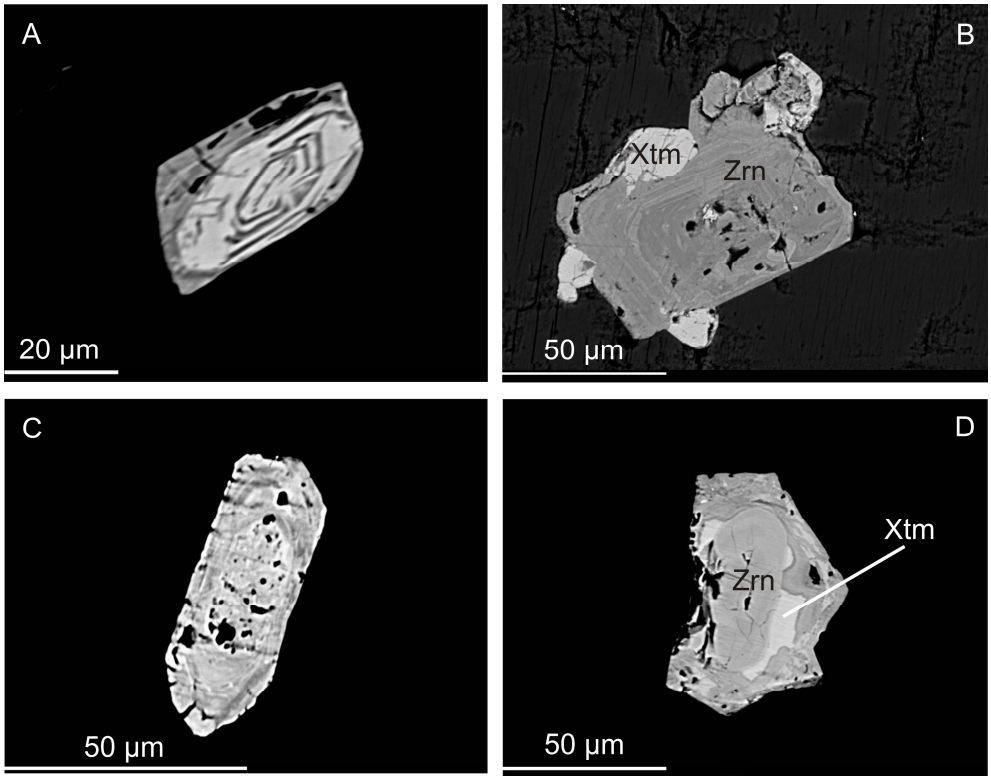

Figure 5 High contrasts BSE image of zircon (Zrn) and xenotime (Xtm) from granites of the Krudum granite body.

4.3.2. Monazite composition

Monazite strongly favours LREE to HREE and Y. In analysed samples the sum of LREE (La + Ce + Pr + Nd + Sm) ranges between 0.21 and 0.94 apfu (atoms per formula unit), being higher in the high-F muscovite-biotite granites (vi) (0.69–0.94) (Table 1). Cerium is, in all cases, the most abundant REE, varying between 7.95 wt. % Ce_2O_3 and 32.57 wt. % Ce_2O_3

Peer-reviewed version available at Minerals 2018, 8, 287; doi:10.3390/min8070287

(0.12–0.48 apfu Ce). The second most abundant REE is La (2.06–15.44 wt. % La_2O_3; 0.03–0.23 apfu La), followed by Nd (2.05–12.04 wt. % Nd_2O_3; 0.03–0.17 apfu Nd), Pr (1.80–3.49 wt. % Pr_2O_3; 0.03–0.05 apfu Pr) and Sm (1.44–3.48 wt. % Sm_2O_3; 0.02–0.05 apfu Sm). Thus, all analysed monazite grains should be termed monazite-(Ce). However, the ranges in atomic ratios between individual LREE vary considerably: the $(La/Nd)_{CN}$ ratio between 0.46 and 3.39, the $(La/Sm)_{CN}$ ratio between 0.49 and 6.27.

The content of Y in analysed monazites ranges from 0.07 to 4.26 wt. % Y_2O_3 (0.00–0.09 apfu Y). The HREE contents are much lower than those of LREE and Y. The concentrations of ΣHREE (Gd + Dy + Er) in analysed monazites range from 0.00 to 0.05 apfu. The concentrations of Th vary between 2.71 and 35.42 wt. % ThO_2 (0.03–0.33 apfu Th). The concentrations of U ranged between 0.19 and 4.54 wt. % UO_2 (0.00–0.04 apfu U).

Two main coupled substitution mechanisms have been proposed for monazite [1, 24–25], namely the cheralite and huttonite substitutions. In the (Th + U + Si) vs. (P + Y + REE) diagram, analysed monazites of all magmatic suites from the KGB plot among the cheralite substitution vector.

However, for monazites from the low-F biotite granites is the huttonite substitution significant (Figure 6).

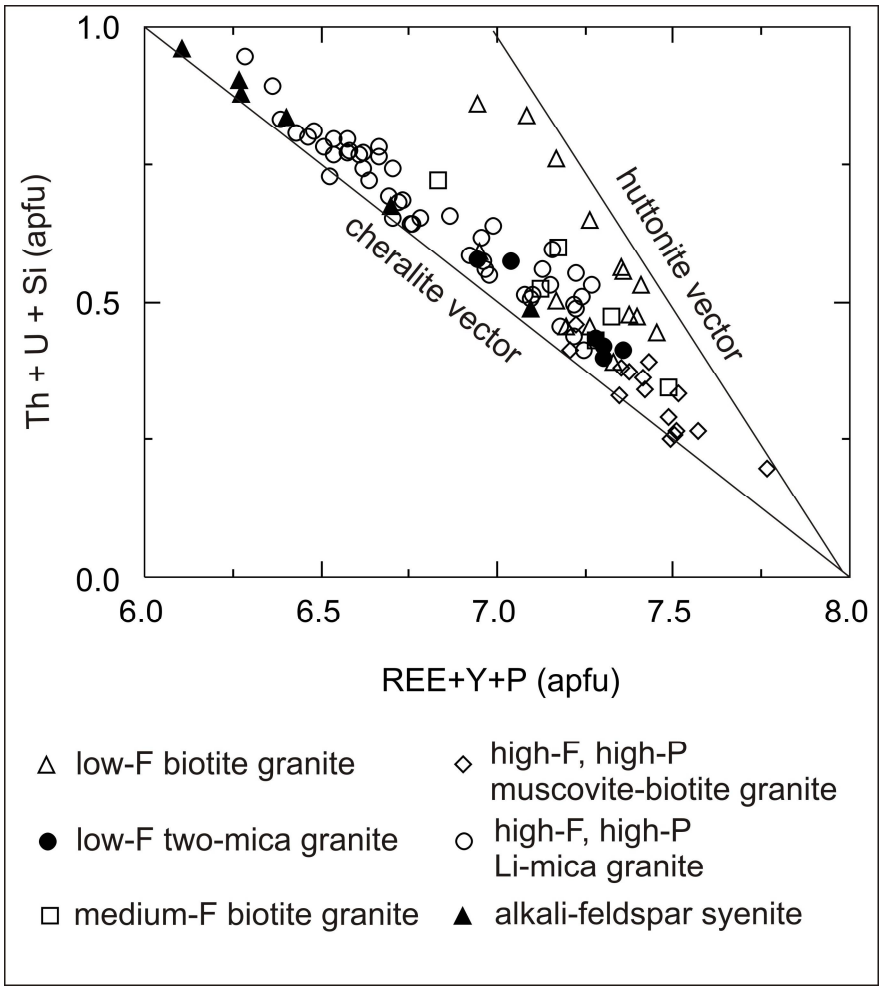

Figure 6 Monazite composition vectors of monazites from the Krudum granite body.

Peer-reviewed version available at Minerals 2018, 8, 287; doi:10.3390/min8070287

The highest fractions of the cheralite component were found in monazites from the high-F, high P_2O_5 granites (iii, iv) (up to 45.6 mol. %) and from the alkali-feldspar syenites (vii) (up to 69.3 mol. %). Similarly, the concentration of the xenotime (YPO_4) component is relatively high in monazites from the high-F, high-P_2O_5 granites (iii, iv) (up to 9.1 mol. %) and from the alkali-feldspar syenites (vii) (up to 9.4 mol. %).

4.3.3. Xenotime composition

The proportion of YPO_4, the main component in xenotime, ranges from 70.66 to 83.75 mol. % (Table 2). Some microprobe analyses reveal low totals suggesting significant hydration of xenotime. The water content estimated from analytical data ranges from 5 to 11 wt. % H_2O. In slightly greisenised high-F, high-P_2O_5 Li-mica granites from the Hub stock the F content it reaches up to 1.12 wt. %. Analysed xenotimes are commonly enriched in HREE (9.3– 19.5 wt. % $HREE_2O_3$), U and Th. The concentrations of Dy and Yb range from 3.05 to 7.67 wt. % Dy_2O_3 (0.035–0.084 apfu Dy) and 2.24 to 8.04 wt. % Yb_2O_3 (0.025–0.088 apfu Yb). The concentrations of U and Th in analysed xenotimes range from 0.45 to 5.55 wt. % UO_2 (0.004–0.044 apfu U) and 0.04-1.73 wt. % ThO_2 (0.000–0.014 apfu Th). Two charge balancing coupled substitutions involving Si (thorite-

coffinite exchange) and/or Ca (cheralite exchange) for the replacement of Y and REE by U and Th are observed in xenotime. In the high-F, Li-mica granites both substitutions mechanisms occur (Figure 7). In some cases the xenotimes are enriched in Sc (up to 2.03 wt.% Sc_2O_3; 0.25 apfu Sc), Zr (up to 1.62 wt. % ZrO_2; 0.03 apfu Zr) and Bi (up to 0.07 wt. % Bi_2O_3; 0.002 apfu Bi) (Figure 7). The Sc and Bi contents show a lack of correlation with other cations in the octahedral position. The Zr content shows a negative correlation with content of Y.

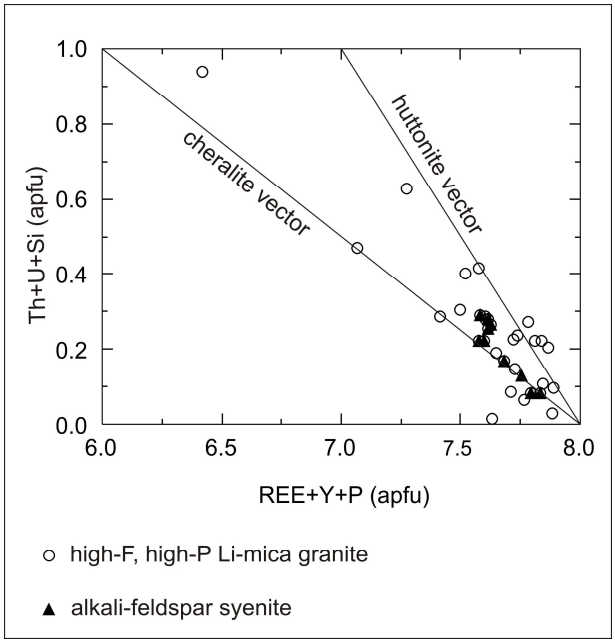

Figure 7 Xenotime composition vectors of xenotimes from the Krudum granite body.

Peer-reviewed version available at Minerals 2018, 8, 287; doi:10.3390/min8070287

4.3.4 Zircon composition

Zircons from the high-F, Li-mica granites (iii, iv) are often hydrated and fluorised. The concentrations of F in zircon from partly greisenised high-F, Li-mica granites reaches up to 1.2 wt. % (0.26 apfu F). Analysed zircons contain moderate Hf concentrations (1.0–4.7 wt. % HfO_2; 0.010–0.047 apfu Hf) (Table 3, Figure 8). The proportion of the hafnium end member indicated by atomic ratio Hf/(Zr + Hf) varies from 0.01 to 0.05. The highest concentrations of HfO_2 were found in zircons from the high-F, Li-mica granites (1.2–4.7 wt. % HfO_2) and from the alkali-feldspar syenites (vii) (1.3–4.1 wt. % HfO_2). In the zircons from the medium-F biotite granites (v) and the high-F, high-P_2O_5 muscovite-biotite granites (vi) HfO_2 concentrations are distinctly lower (1.0–2.5 wt. %). In the zircons from the alkali-feldspar syenites (vii) enrichment in P was observed, which is not associated with a simultaneous enrichment in Y + REE. The high concentration of P (up to 8.29 wt. % P_2O_5; 0.24 apfu P) is usually accompanied by enrichment of Ca (up to 3.9 wt. % CaO; 0.14 apfu Ca) and Al (0.02–2.0 wt. % Al_2O_3; 0.00–0.08 apfu Al). Analysed zircons from the high-F, high-P_2O_5 granites (iii, iv) are also enriched in the Y (up to 5.5 wt. % Y_2O_3; 0.10 apfu Y) and Sc (up to 1.17 wt. % Sc_2O_3; 0.03 apfu Sc). These

Peer-reviewed version available at Minerals 2018, 8, 287; doi:10.3390/min8070287

altered zircons are also enriched in Bi (up to 5.16 wt. % Bi_2O_3, 0.033 apfu Bi). The zircons from the medium-F biotite granites (v) and from the high-F muscovite-biotite granites (vi) displays distinctly lower concentrations of Y (0–0.8 wt. % Y_2O_3), Sc (0–0.4 wt. % Sc_2O_3) and Bi (0.05–0.14 wt. % Bi_2O_3). The uranium and thorium are ubiquitous components all analysed zircons, especially in the altered zircons from high-F, high-P_2O_5 Li-mica granites. In these granites concentrations of U up to 3.1 wt. % UO_2 (0.02 apfu U) were found. The concentrations of Th in altered zircons from high-F, high-P_2O_5 Li-mica granites are between 0.2 and 1.7 wt. % ThO_2 (0.002–0.013 apfu Th). The concentrations of U and Th in the medium-F biotite granites and in the high-F, high-P_2O_5 muscovite-biotite granites are lower (0.04–0.65 wt. % UO_2; 0.01–0.21 wt. % ThO_2).

5. Discussion

5.1. Substitution in monazite

Two main coupled substitutions mechanisms have been proposed for monazite, cheralite substitution $(Th, U)^{4+} + Ca^{2+} = 2\ REE^{3+}$ and huttonite substitution $(Th, U)^{4+} + Si^{4+} = REE^{3+} + P^{5+}$[24–28]. For the analysed monazite from all granitic suites of the KGB the cheralite substitution is more common. The predominance of the cheralite substitution over the

huttonite substitution was also found in other highly fractionated high-F, Li-mica granites from other parts of the Krušné Hory/Erzgebirge batholith and the Fichtelgebirge granites in NE Bavaria, Germany [2, 8, 24]. High contents of the cheralite component (> 20-30 mol. %) were also found in highly fractionated S-type granites from the West Carpathian belt [1] and in similar S-type granites from the Belvís de Monroy pluton in the Iberian Variscan belt [6].

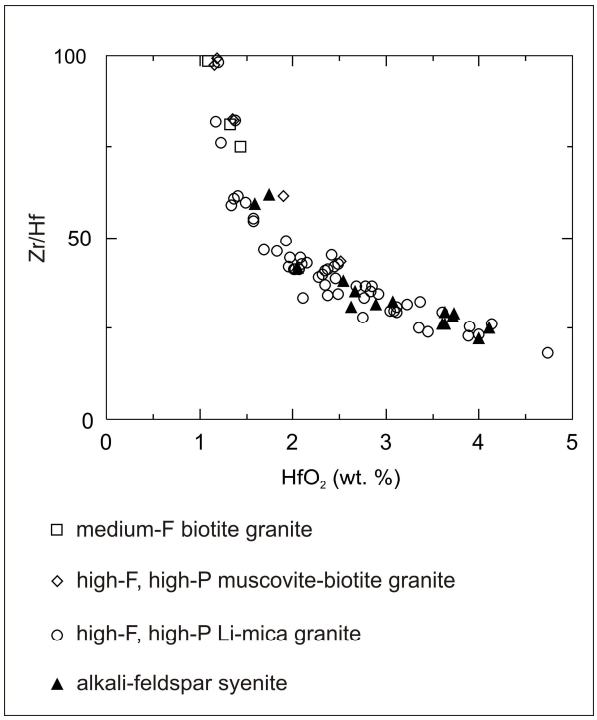

Figure 8 Chemical composition of zircon from granites of the Krudum granite body.

Peer-reviewed version available at Minerals 2018, 8, 287; doi:10.3390/min8070287

5.2. Substitution in xenotime

Like for monazite, two main mechanisms exist for the replacement of Y by REE, U and Th in xenotime: charge balancing coupled substitutions involving Si and Ca (thorite-coffinite-type and cheralite-type substitutions respectively) [1, 4, 29–30]. In the analysed xenotimes from high-F, high P_2O_5 granites (iii, iv) both substitutions mechanisms exist. Both were also previously found in the S-type, high-F, Li-mica granites from the German part of Krušné Hory/Erzgebirge area [29]. However, according to Pérez-Soba et al. [6], unlike zircon, xenotime from highly fractionated peraluminous granites from the Belvís de Monroy pluton in the Iberian Variscan belt showed predominance of one substitution, the cheralite substitution, over the thorite-coffinite substitution.

5.3. Substitution in zircon

The entry of Y + HREE and P into the zircon structure is usually explained via xenotime substitution, whereas zircon and xenotime are isostructural [30–32]. The uranium and thorium in zircon cause its metamictization, which is usually followed by hydration (replacement of O^{2-} by OH^-) and fluoritization [33]. The apparent surplus on the A-site could be explained by occurring substantial amounts of interstitial cations (e.g., Fe, Ca, Al, As, Bi,

Sc) [34–35]. For enrichment of the Sc in zircon the pretulite ($ScPO_4$) exchange is usually suggested [36]. The moderate to strong deviation of altered zircons from stoichiometry was also found in some other occurrences of the high-F, Li-mica granites in the Krušné Hory/Erzgebirge area (e.g. Cínovec, Podlesí, Altenberg, Seifen) [30, 37–39] and in some other occurrences of altered zircon worldwide [40–46].

6. Conclusion

The Krudum granite body represents highly fractionated granitic rocks from the medium-F biotite granites to the high-F, high-P_2O_5 Li-mica granites. All these granite varieties contain variable concentrations of monazite and zircon. Xenotime was found only in the high-F, high-P_2O_5 Li-mica granites and in the alkali-feldspar syenites.

All analysed monazites of all magmatic suites from the KGB displayed strong preference of cheralite substitution, with the highest amounts of the cheralite component found in monazites from the high-F, high P_2O_5 Li-mica granites (up to 45.6 mol. %) and from the alkali-feldspar syenites (up to 69.3 mol. %). For monazites from the low-F biotite granites of the Karlovy Vary pluton the huttonite substitution is significant.

Peer-reviewed version available at Minerals 2018, 8, 287; doi:10.3390/min8070287

The proportion of YPO_4 in all analysed xenotimes ranges from 71 to 84 mol. %. Some microprobe analyses reveal low totals, suggesting significant hydration of xenotime. The water content estimated from analytical data ranges in these xenotimes from 5 to 11 wt. % H_2O. In slightly greisenised high-F Li-mica granites from the Hub stock the F content it reaches up to 1.12 wt. %. Analysed xenotimes are commonly enriched in the HREE (9.3–19.5 wt. % $HREE_2O_3$), U and Th. In analysed xenotimes two charge balancing coupled substitutions involving Si (thorite-coffinite exchange) and/or Ca (cheralite exchange) for the replacement of Y and REE by U and Th were found.

Analysed zircons from analysed granite suites contain rather moderate Hf concentrations (1.0–4.7 wt. % HfO_2; 0.010–0.047 apfu Hf). The highest concentrations of HfO_2 were found in zircons from the high-F Li-mica granites (1.2–4.7 wt. % HfO_2) and from the alkali-feldspar syenites (1.3–4.1 wt. % HfO_2). Zircons from the high-F Li-mica granites are often hydrated and fluorised. The concentrations of F in zircon from partly greisenised high-F Li-mica granites reaches up to 1.2 wt. % (0.26 apfu F). In zircons from the alkali-feldspar syenites was observed enrichment in P, which is not associated with a simultaneous enrichment in Y + REE. The high

concentration of P (up to 8.29 wt. % P_2O_5; 0.24 apfu P) is usually accompanied by enrichment of Ca (up to 3.9 wt. % CaO; 0.14 apfu Ca) and Al (0.02–2.0 wt. % Al_2O_3; 0.00–0.08 apfu Al). Analysed zircons from the high-F Li-mica granites are enriched in Y (up to 5.5 wt. % Y_2O_3; 0.10 apfu Y) and Sc (up to 1.17 wt. % Sc_2O_3; 0.03 apfu Sc). These altered zircons are also enriched in Bi (up to 5.16 wt. % Bi_2O_3, 0.033 apfu Bi).

Acknowledgments: The research for this paper was carried out thanks to the support of the long-term conceptual development research organisation RVO 67985891. P. Gadas and R. Škoda from the Masaryk University, Brno are thanked for their assistance during the microprobe work. I wish also to thank A. Szameitat for her constructive remarks and English corrections.

Conflicts of Interest: The author declares no conflict of interest.

References

[1] Broska, I.; Petrík, I. Genesis and stability of accessory phosphates in silicic magmatic rocks: a Western Carpathian case study. *Mineralogia* **2008**, *39*, 53–65.

[2] Förster, H.J.; Rhede, D.; Hecht, L. Chemical composition of radioactive accessory minerals: implications for the evolution, alteration, age, and uranium fertility of the Fichtelgebirge granites (NE Bavaria, Germany).

Neu. Jb. Mineral., Abh. **2008**, *185*, 161–182. DOI:10.1127/0077-7757/2008/0117

[3] Harlov, D. E.; Procházka, V.; Förster H. J.; Matějka D. Origin of monazite-xenotime-zircon-fluorapatite assemblages in the peraluminous Melechov granite massif, Czech Republic. *Mineral. Petrol.* **2008**, *94*, 9–26. DOI:10.1007/s00710-008-0003-8

[4] Hetherington, C. J.; Jercinovic, M. J.; Williams, M. L.; Mahan, K. Understanding geologic processes with xenotime: Composition, chronology, an a protocol for electron probe microanalysis. *Chem. Geol.* **2008**, *254*, 133–147. DOI:10.1016/j.chemgeo.2008.05.020

[5] Kelts, A. B.; Ren, M.; Anthony, E. Y. Monazite occurrence, chemistry, and chronology in the granitoid rocks of the Lachlan Fold Belt, Australia: An electron microprobe study. *Am. Mineral*. **2008**, *93*, 373–383.

[6] Pérez-Soba, C.; Villaseca, C.; Orejana, D.; Jeffries, T. Uranium-rich accessory minerals in the peraluminous and perphosphorous Belvís de Monroy pluton (Iberian Variscan belt). *Contrib. Mineral. Petro*l. **2014**, *167*, DOI 10.1007/s00410-014-1008-4.

[7] Uher, P.; Kohút, M.; Ondrejka, M.; Konečný, P.; Siman, P. Monazite-(Ce) in Hercynian granites and pegmatites of the Bratislava massif, Western Carpathians: compositional variations and Th-U-Pb electron-microprobe dating. *Acta Geol. Slov.* **2014**, *6*, 215–231.

[8] Breiter, K. Monazite and zircon as major carriers of Th, U, and Y in peraluminous granites: examples from the Bohemian Massif. *Mineral. Petrol.* **2016**, *110*, 767–785. DOI:10.1007/s00710-016-0448-0

[9] Förster, H. J.; Tischendorf, G.; Trumbull, R. B.; Gottesmann, B. Late-collisional granites in the Variscan Erzgebirge (Germany). *J. Petrol.* **1999**, *40*, 1613–1645. DOI:10.1093/petroj/40.11.1613

[10] Förster, H. J.; Romer, R. L. Carboniterous magmatism. In *Pre-Mesozoic Geology of Saxo-Thuringia – From the Cadomian Active Margin to the Variscan Orogen*; Linnemann, U.; Romer, R. L., Eds.; Schweizerbart Verlag Stuttgart, Germany, 2010; pp. 287–308.

[11] Blecha, V.; Štemprok, M. Petrochemical and geochemical characteristics of late Variscan granites in the Karlovy Vary Massif (Czech Republic) – implications for gravity and magnetic interpretation at shallow depths. *J. Geosci.* **2012**, *57*, 65–85. DOI:10.3190/jgeosci.115

[12] Hofmann, Y.; Jahr, T.; Jentzch, G. Three-dimensional gravimetric modelling to detect deep structure of the region Vogtland/NW Bohemia. *J. Geodyn.* **2003**, *35*, 209–220. DOI:10.1016/s0264-3707(02)00063-7

[13] Finger, F.; Gerdes, A.; René, M.; Riegler, G. The Saxo-Danubian granite belt: Magmatic response to post-collisional delamination of mantle lithosphere below the south-western sector of the Bohemian Massif (Variscan orogen). *Geol. Carpath.* **2009**, *60*, 205–212. DOI:10.2478/v10096-009-0014-3

[14] Tichomirova, M.; Leonhardt, D. New age determinations (Pb-Pb zircon evaporation, Rb/Sr) on the granites from Aue-Schwarzenberg and Eibenstock, Western Erzgebirge, Germany. *Z. Geol. Wiss.* **2010**, *38*, 99–123.

[15] Dolejš, D.; Bendl, J.; Štemprok, M. Rb-Sr isotopic composition in the Western Krušné hory/Erzgebirge pluton, Central Europe: record of variations in source lithology, mafic magma input and postmagmatic hydrothermal events. *Mineral. Petrol.* **2016**, 110, 601–622. DOI:10.007/s00710-016-0434-6

[16] Breiter, K.; Förster, H. J.; Seltmann, R. Variscan silicic magmatism and related tin-tungsten mineralization on the Erzgebirge-Slavkovský les metallogenic province. *Miner. Deposita* **1999**, *34*, 505–521. DOI:10.1007/s001260050217

[17] Jarchovský, T. The nature and genesis of greisen stocks at Krásno, Slavkovský les area – western Bohemian, Czech Republic. J. *Czech Geol. Soc.* **2006**, *51*, 201–216.

[18] René, M.; Škoda, R. Nb-Ta-Ti oxides fractionation in rare-metal granites: Krásno-Horní Slavkov ore district, Czech Republic. *Mineral. Petrol.* **2011**, *103*, 37–48. DOI:10.1007/s00710-011-0152-z

[19] Dolníček, Z.; René, M. Prochaska, W.; Kovář, M. Fluid evolution of the Hub stock, Horní Slavkov-Krásno Sn-W ore district, Bohemian Massif, Czech Republic. *Miner. Deposita* **2012**, *47*, 821–833. DOI:10.1007/s00126-012-0400-0

[20] René, M. Petrology, geochemistry and mineralogy of greisens associated with tin-tungsten mineralisation: Hub stock deposit at Krásno-Horní Slavkov ore district, Czech Republic. In *Contributions to mineralisation*; Al-Juboury A.I. Ed. InTech: Rijeka, Croatia, 2018; pp. 1–22.

Peer-reviewed version available at Minerals 2018, 8, 287; doi:10.3390/min8070287

[21] Pouchou, J. L.; Pichoir, F. „PAP“ (φ-ρ-Z) procedure for improved quantitative microanalysis. In *Microbeam Analysis*; Armstrong J. T. Ed. San Francisco Press: San Francisco, USA, 1985; pp. 104–106.

[22] Pyle, J. M.; Spear, M. S.; Rudnick, R. L.; McDonough, W.F. Monazite-xenotime-garnet equilibrium in metapelites and a new monazite-garnet thermometer. *J. Petrol*. **2001**, *42*, 2083–2107. DOI:10.1093/petrology/42.11.2083

[23] Chappell, B. W.; Hine, R. The Cornubian batholith: an example of magmatic fractionation on a crustal scale. *Res. Geol*. **2006**, *56*, 203–244. DOI:10.1111/j.1751-3928.2006.tb00281.x

[24] Förster, H. J. The chemical composition of REE-Y-Th-U-rich accessory minerals in peraluminous granites of the Erzgebirge-Fichtelgebirge region, Germany. Part I: The monazite-(Ce)-brabantite solid solutions series. *Am. Mineral.* **1998**, *83*, 259–272.

[25] Hoshino, M.; Watanabe, Y.; Ishihara, S. Crystal chemistry of monazite from the granitic rocks of Japan: Petrogenetic implications. *Can. Mineral.* **2012**, *50*, 1331–1346. DOI:10.3749/canmin.50.5.1331

[26] Gramaccioli, C. M.; Segalstad, T. V. A uranium- and thorium-rich monazite from a south-alpine pegmatite at Piona, Italy. *Am. Mineral.* 1**978**, *63*, 757–761.

[27] Franz, G.; Andrehs, G.; Rhede, D..Crystal chemistry of monazite and xenotime from Saxothuringian-Moldanubian metapelites, NE Bavaria, Germany. *Eur. J. Min*. **1996**, *8*, 1097–1118.

[28] Linthout, K. Tripartite division of the system $2REEPO_4$-$CaTh(PO_4)_2$-$2ThSiO_4$, dicreditation of brabantite, and recognition of cheralite as a name for members dominated by $CaTh(PO_4)_2$. *Can. Mineral*. **2007**, *45*, 503–508. DOI:10.2113/gscanmin.45.3.503

[29] Förster, H. J. The chemical composition of REE-Y-Th-U-rich accessory minerals in peraluminous granites of the Erzgebirge-Fichtelgebirge region, Germany. Part II: Xenotime. *Am. Mineral*. **1998**, *83*, 1302–1315.

[30] Förster, H. J. Composition and origin of intermediate solid solutions in the system thorite-xenotime-zircon-coffinite. *Lithos* **2006**, *88*, 35–55. DOI: 10.1016/j.lithos.2005.08.003

[31] Hata, S. Xenotime and variety of zircon from Iisaka. *Sci. Pap. Inst. Chem. Res*. **1938**, *34*, 619–622

[32] Uher, P.; Černý, P. Zircon in Hercynian granitic pegmatites of the Western Carpathians, Slovakia. *Geol. Carpath*. **1998**, *49*, 261–270.

[33] Geisler, T.; Rashwan, A. A.; Rahn, A.K.; Poller, U.; Zwingmann, H.; Pidgeon, R. T.; Schleicher, H.; Tolmaschek, F. Low-temperature hydrothermal alteration of natural metamict zircons from the Eastern Desert Egypt. *Mineral. Mag.* **2003**, *67*, 485–508. DOI:10.1180/0026461036730112

[34] Hoskin, P. W. O.; Kinny, P. D.; Wyborn, D.; Chappell, B. W. Identifying accessory mineral saturation during differentiation in granitoid magmas: an integrated approach. *J. Petrol*. **2000**, *41*, 1365–1396. DOI:10.1093/petrology/41.9.1365

[35] Finch, R. J.; Hanchar, J. M. Structure and chemistry of zirocn and zircon group minerals. In *Zircon*. Hanchar, J. M.; Hoskin, P. W. O. eds. *Reviews in mineralogy and geochemistry* **2003**, *53*, 1–26.

[36] Bernhard, F.; Walter, F.; Ettinger, K.; Taucher, J.; Mereiter, K. Pretulite. $ScPO_4$: a new scandium mineral from the Styrian and lower Austrian lazulite occurrences, Austria. *Am. Mineral*. **1998**, *83*, 625–630.

[37] Johan, Z.; Johan, V. Accessory minerals of the Cínovec (Zinnwald) granite cupola, Czech Republic. Part 1: Nb-, Ta- and Ti-bearing oxides. *Mineral. Petrol*. **2005**, *83*, 113–150. DOI:10.1007/s00710-004-0058-0

[38] Breiter, K.; Förster, H. J.; Škoda, R. Extreme P-. Bi-, Nb-, Sc-, U- and F-rich zircon from fractionated perphosphorus granites: the peraluminous Podlesí granite system, Czech Republic. *Lithos* **2006**, *88*, 15–34. DOI:10.1017/j.lithos.2005.08.011

[39] Förster, H. J.; Rhede, D. The Be-Th-rich granite of Seiffen (eastern Erzgebirge, Germany): accessory-mineral chemistry, composition, and age of late-Variscan Li-F granite of A-type affinity. *N. Jb. Mineral., Abh*. **2006**, *182*, 307–321. DOI:10.1127/0077-7757/2006/0055

[40] Pointer, C. M.; Ashworth, J. R.; Ixer, R. A. The zircon-thorite mineral group in metasomatized granite, Ririwai, Nigeria 1. Geochemistry and metastable solid solution in thorite and coffinite. *Mineral. Petrol*. **1988**, *38*, 245–262. DOI:10.1007/BF01167091

[41] Smith, D. G. W.; De St, J. L.; Reed, S. J. B.; Long, J. V. P. Zonally metamictized and other zircon from Thor Lake, Northwest Territories. *Can. Mineral.* **1991**, *29,* 301–309.

[42] Peréz-Soba, C.; Villaseca, C.; Gonzáles del Tánago, J. The composition of zircon in the peraluminous Hercynian granites of the Spanish Central System batholith. *Can. Mineral*. **2007**, *45*, 509–527. DOI:10.2113/gscanmin.45.3509

[43] Anderson, A. J.; Wirth, R.; Thomas, R. The alteration of metamict zircon and its role in the remobilization of high-field-strength elements in the Georgeville granite, Nova Scotia. *Can. Mineral.* **2008**, *46*. 1–18. DOI:10.3749/canmin.46.1.1

[44] Abd El-Naby, H. H. High and low temperature alteration of uranium and thorium minerals, Um Ara granites, south Eastern Desert, Egypt. *Ore Geol. Rev.* **2009**, *35*, 436–446. DOI:10.1016/j.oregeorev.2009.02.006

[45] Nasdala, L.; Kronz, A.; Wirth, R.; Vászi, T.; Pérez-Soba, C.; Willner, A.; Kennedy, A.K. The phenomenon of different electron microprobe totals in radiation-damaged and altered zircon. *Geochim. Cosmochim. Acta* **2009**, *73*, 1637–1650. DOI:10.1016/j.gca.2008.12.010

[46] Hoshino, M.; Kimata, M.; Nishida, N., Shimizu, M.; Akasaka, T. Crystal chemistry of zircon from granitic rocks, Japan: genetic

implications of HREE, U and Th enrichment. *N. Jb. Mineral., Abh.* **2010**, *187*, 167–188. DOI:10.1127/0077-7757/2010/0177

Table 1 Representative EPMA of monazite

Sample	KRU-34	KRU-35	1162-2	1162-13	1008-33	1283-17	1542-10
Variety wt%	medium-F granite	medium-F granite	high-F two-mica granite	high-F two-mica granite	high-F Li-mica granite	high-F Li-mica granite	alkali-feldspar syenite
P_2O_5	29.27	29.09	29.22	28.12	28.70	31.19	29.65
SiO_2	0.62	0.75	0.58	0.55	1.15	0.48	0.67
ThO_2	8.23	10.33	5.81	2.71	10.08	15.13	19.68
UO_2	0.93	0.88	1.23	0.19	0.31	1.68	3.00
Y_2O_3	2.13	2.53	2.91	0.38	3.38	2.26	1.80
La_2O_3	11.68	11.36	11.51	15.44	10.47	7.73	6.60
Ce_2O_3	26.29	24.73	26.17	32.57	25.22	21.45	17.49
Pr_2O_3	2.80	2.77	3.03	3.49	2.95	2.63	2.20
Nd_2O_3	10.02	9.48	11.36	12.04	10.60	8.87	7.90
Sm_2O_3	1.79	1.81	2.54	1.88	2.25	2.29	2.68
Gd_2O_3	1.20	1.12	1.95	0.72	1.83	1.50	1.65
Dy_2O_3	0.80	0.80	1.02	0.11	1.14	1.02	0.88
Er_2O_3	0.17	0.17	0.21	0.03	0.23	0.12	0.14
CaO	1.30	1.75	1.53	0.32	1.29	3.29	4.93
PbO	0.17	0.17	0.16	0.04	0.14	0.28	0.35
Total	97.40	97.74	99.23	98.59	99.74	99.92	99.62
apfu, O=4							
P	0.986	0.977	0.973	0.960	0.955	1.004	0.976
Si	0.025	0.030	0.023	0.022	0.045	0.018	0.026
Th	0.075	0.093	0.052	0.025	0.090	0.131	0.174
U	0.008	0.008	0.011	0.002	0.003	0.014	0.026
Y	0.045	0.053	0.061	0.008	0.071	0.046	0.037
La	0.171	0.166	0.167	0.230	0.152	0.108	0.095
Ce	0.383	0.359	0.376	0.481	0.363	0.298	0.249
Pr	0.041	0.040	0.043	0.051	0.042	0.036	0.031

Peer-reviewed version available at *Minerals* **2018**, *8*, 287; doi:10.3390/min8070287

Nd	0.142	0.134	0.159	0.173	0.149	0.120	0.110
Sm	0.025	0.025	0.034	0.026	0.030	0.030	0.036
Gd	0.016	0.015	0.025	0.010	0.024	0.019	0.021
Dy	0.010	0.010	0.013	0.001	0.014	0.012	0.011
Er	0.002	0.002	0.003	0.000	0.003	0.001	0.002
Ca	0.055	0.074	0.064	0.014	0.054	0.134	0.205
Pb	0.002	0.002	0.002	0.000	0.001	0.003	0.004
$LREEPO_4$	0.7758	0.7312	0.7633	0.9397	0.7308	0.6095	0.5026
$HREEPO_4$	0.0295	0.0282	0.0420	0.0111	0.0424	0.0347	0.0352
$CaTh(PO_4)_2$	0.1158	0.1548	0.1311	0.0281	0.1118	0.2907	0.4249
$ThSiO_4$	0.0316	0.0303	0.0010	0.0131	0.0414	0.0152	0.0000
YPO_4	0.0474	0.0554	0.0625	0.0080	0.0735	0.0499	0.0383

Table 2 Representative EPMA of xenotime

Sample	1007-4	1007-11	1007-19	997-9	1542-18	1542-20
Variety wt%	high-F Li-mica granite	high-F Li-mica granite	high-F Li-mica granite	alkali-feldspar syenite	alkali-feldspar syenite	alkali-feldspar syenite
P_2O_5	34.50	36.31	33.87	31.99	32.75	33.00
SiO_2	0.96	b.d.l.	0.85	0.23	0.97	0.93
ThO_2	0.87	0.04	0.72	0.53	1.50	1.29
UO_2	4.43	0.93	4.56	2.49	3.06	2.97
Y_2O_3	38.83	48.50	38.23	39.59	40.18	40.19
La_2O_3	b.d.l.	0.03	0.01	b.d.l.	b.d.l.	0.01
Ce_2O_3	b.d.l.	b.d.l.	0.03	0.04	0.11	0.14
Pr_2O_3	b.d.l.	0.02	0.07	0.10	0.08	0.05
Nd_2O_3	0.32	0.08	0.42	0.26	0.38	0.44
Sm_2O_3	0.87	0.11	0.79	0.84	0.67	0.68
Gd_2O_3	2.56	0.61	2.38	2.72	2.29	2.21
Dy_2O_3	7.59	3.79	7.35	6.69	6.16	6.19
Ho_2O_3	0.98	0.69	1.06	b.d.l.	b.d.l.	b.d.l.
Er_2O_3	3.23	2.48	3.42	3.15	3.45	3.43
Yb_2O_3	4.23	3.81	3.96	4.50	2.31	2.36
Lu_2O_3	0.81	0.56	0.91	0.02	b.d.l.	b.d.l.
CaO	0.42	0.89	0.51	0.49	0.19	0.16
PbO	0.18	0.02	0.10	0.43	0.51	0.51
F	0.09	1.12	0.10	0.05	0.10	0.02
O=F	0.04	0.47	0.04	0.02	0.04	0.01
Total	100.83	99.52	99.30	94.10	94.67	94.57
apfu, O=4						
P	0.985	1.001	0.984	0.973	0.974	0.978
Si	0.032	0.000	0.029	0.008	0.034	0.033
Th	0.007	0.000	0.006	0.004	0.012	0.010
U	0.033	0.007	0.035	0.020	0.024	0.023
Y	0.696	0.840	0.697	0.756	0.750	0.748
La	0.000	0.000	0.000	0.000	0.000	0.000
Ce	0.000	0.000	0.000	0.001	0.001	0.002

Peer-reviewed version available at Minerals 2018, 8, 287; doi:10.3390/min8070287

Pr	0.000	0.000	0.001	0.001	0.001	0.001
Nd	0.004	0.001	0.005	0.003	0.005	0.005
Sm	0.010	0.001	0.009	0.010	0.008	0.008
Gd	0.029	0.007	0.027	0.032	0.027	0.026
Dy	0.082	0.040	0.081	.0.077	0.070	0.070
Ho	0.010	0.007	0.012	0.000	0.000	0.000
Er	0.034	0.025	0.037	0.036	0.038	0.038
Yb	0.043	0.038	0.041	0.049	0.025	0.025
Lu	0.008	0.006	0.009	0.000	0.000	0.000
Ca	0.015	0.031	0.019	0.019	0.007	0.006
Pb	0.002	0.000	0.001	0.004	0.005	0.005
F	0.019	0.231	0.022	0.011	0.022	0.004
$LREEPO_4$	0.0144	0.0020	0.0153	0.0148	0.0154	0.0165
$HREEPO_4$	0.2117	0.1226	0.2112	0.1917	0.1644	0.1644
$CaTh(PO_4)_2$	0.0308	0.0616	0.0388	0.0375	0.0144	0.0124
$ThSiO_4$	0.0270	0.0000	0.0230	0.0090	0.0340	0.0320
YPO_4	0.7153	0.8375	0.7112	0.7470	0.7708	0.7735

b.d.l. – below detection limit

Table 3 Representative EPMA of zircon

Sample	23-44	23-45	1162-5	1250-27	1007-2	1280-2	997-1	1542-1
Variety wt%	medium-F granite	medium-F granite	high-F two-mica granite	high-F two-mica granite	high-F Li-mica granite	high-F Li-mica granite	alkali-feldspar syenite	alkali-feldspar syenite
SiO_2	31.60	32.16	31.85	32.30	31.49	32.12	32.32	31.09
Al_2O_3	b.d.l.	b.d.l.	b.d.l.	b.d.l.	b.d.l.	0.03	0.01	0.12
ZrO_2	64.19	65.40	63.05	66.00	61.73	63.99	65.32	62.47
HfO_2	1.43	1.03	2.52	1.36	3.60	3.37	1.33	3.71
CaO	0.01	0.03	0.05	b.d.l.	0.03	0.02	0.04	0.18
FeO	b.d.l.	b.d.l.	0.05	0.02	0.16	0.07	0.02	0.54
MnO	0.02	b.d.l.	0.02	b.d.l.	0.04	0.01	0.02	0.00
MgO	b.d.l.	0.01	0.01	0.02	b.d.l.	b.d.l.	0.01	0.01
P_2O_5	0.50	0.05	0.59	0.02	0.79	0.07	0.38	1.02
Sc_2O_3	0.11	b.d.l.	0.35	b.d.l.	0.31	0.05	0.09	0.56
As_2O_5	b.d.l.	b.d.l.	0.01	0.05	0.10	0.04	0.04	0.13

Peer-reviewed version available at *Minerals* **2018**, *8*, 287; doi:10.3390/min8070287

Bi_2O_3	0.09	0.08	0.05	0.10	0.07	0.07	0.09	0.13
Y_2O_3	0.48	0.23	0.26	b.d.l.	0.38	b.d.l.	0.20	0.03
La_2O_3	b.d.l.	b.d.l.	b.d.l.	b.d.l.	0.02	b.d.l.	0.02	0.01
Ce_2O_3	b.d.l.	b.d.l.	0.02	b.d.l.	b.d.l.	0.01	0.01	b.d.l.
Pr_2O_3	0.03	b.d.l.	b.d.l.	0.03	b.d.l.	b.d.l.	0.02	b.d.l.
Nd_2O_3	b.d.l.	0.10	b.d.l.	b.d.l.	0.04	0.02	0.08	0.06
Sm_2O_3	0.01	0.01	b.d.l.	0.01	b.d.l.	0.01	b.d.l.	b.d.l.
Gd_2O_3	b.d.l.	0.01	0.01	b.d.l.	b.d.l.	b.d.l.	0.02	0.05
Dy_2O_3	0.03	0.05	0.01	b.d.l.	b.d.l.	0.01	0.02	0.04
Er_2O_3	0.12	0.07	0.02	0.06	0.10	0.06	0.06	0.07
Yb_2O_3	0.21	0.06	0.18	0.03	0.29	0.02	0.05	0.14
UO_2	0.50	0.09	0.65	0.04	0.52	0.13	0.11	0.36
ThO_2	0.01	0.04	0.02	0.02	0.01	0.03	b.d.l.	0.08
PbO	0.02	b.d.l.	0.03	b.d.l.	0.04	b.d.l.	0.01	b.d.l.
F	b.d.l.	b.d.l.	0.03	b.d.l.	b.d.l.	b.d.l.	0.01	0.05
O=F	0.00	0.00	0.01	0.00	0.00	0.00	0.00	0.02
Total	99.36	99.42	99.77	100.06	99.68	100.13	100.28	100.85
apfu, O=4								
Si	0.982	0.995	0.987	0.994	0.981	0.995	0.990	0.960
P	0.013	0.001	0.015	0.001	0.021	0.002	0.010	0.027
Al	0.000	0.000	0.000	0.000	0.000	0.001	0.000	0.004
Σ T-site	0.995	0.996	1.002	0.995	1.002	0.998	1.000	0.991
Zr	0.973	0.987	0.952	0.990	0.938	0.967	0.976	0.892
Hf	0.013	0.009	0.022	0.012	0.032	0.030	0.012	0.034
Ca	0.000	0.001	0.002	0.000	0.001	0.001	0.001	0.006
Fe	0.000	0.000	0.001	0.001	0.004	0.002	0.001	0.014
Mn	0.001	0.000	0.001	0.000	0.001	0.000	0.001	0.000
Mg	0.000	0.000	0.000	0.001	0.000	0.000	0.000	0.000
Sc	0.003	0.000	0.009	0.000	0.008	0.001	0.002	0.015
As	0.000	0.000	0.000	0.001	0.002	0.001	0.001	0.002
Bi	0.000	0.000	0.000	0.001	0.000	0.000	0.000	0.001
Y	0.008	0.004	0.004	0.000	0.006	0.000	0.003	0.000
La	0.000	0.000	0.000	0.000	0.000	0.000	0.000	0.000
Ce	0.000	0.000	0.000	0.000	0.000	0.000	0.000	0.000

Pr	0.000	0.000	0.000	0.000	0.000	0.000	0.000	0.000
Nd	0.000	0.001	0.000	0.000	0.000	0.000	0.001	0.001
Sm	0.000	0.000	0.000	0.000	0.000	0.000	0.000	0.000
Gd	0.000	0.000	0.000	0.000	0.000	0.000	0.000	0.001
Dy	0.000	0.000	0.000	0.000	0.000	0.000	0.000	0.000
Er	0.001	0.001	0.000	0.001	0.001	0.001	0.001	0.001
Yb	0.002	0.001	0.002	0.000	0.003	0.000	0.000	0.001
U	0.003	0.001	0.004	0.000	0.004	0.001	0.001	0.002
Th	0.000	0.000	0.000	0.000	0.000	0.000	0.000	0.001
Pb	0.000	0.000	0.000	0.000	0.000	0.000	0.000	0.000
Σ A site	1.004	1.005	0.997	1.007	1.000	1.004	1.000	0.971
F	0.000	0.000	0.006	0.000	0.000	0.000	0.002	0.010

b.d.l. – below detection limit